J. Fluid Mech. (1972), *vol.* 51, *part* 4, *pp.* 751–771
Printed in Great Britain

Wave-induced wind fluctuation over the sea

By JUNSEI KONDO, YUKIO FUJINAWA AND GEN'ICHI NAITO

Institute of Coastal Oceanology, National Research Center for Disaster Prevention, Hiratsuka, Japan

(Received 4 January 1971 and in revised form 20 September 1971)

Simultaneous measurements of the sea surface displacement and the longitudinal component of the wind velocity at several levels are reported. They were obtained at the Marine Tower under various conditions, with the air and the waves moving either in the same or in opposite directions. The spectral analysis was made. The cross-correlation coefficient between the sea surface displacement and the wind velocity is large at the layer adjacent to the surface and decreases with increasing mean wind velocity and height. Below a certain level which is several times or several tens of times higher than the height of the critical level where the wind velocity component in the direction of wave propagation equals the wave velocity, the phase lag of the Fourier component of the wind velocity compared with the surface elevation component is about 160 to 190°. Above this layer the wave-induced wind component is very weak and the phase reversal takes place at the height where the mean wind velocity equals 1·2 to 1·5C, C being the phase velocity of wave. When the wind blows in the opposite direction from that of the wave propagation, the wind fluctuation is in phase with respect to the wave motion and the amplitude of wave-induced wind component is relatively large. Some discrepancies are shown between the observations and the predictions from the theory of inviscid fluids.

1. Introduction

Wave–wind interaction has important influences on the generation of surface waves and drift current as well as on the transfer of heat and mass through the interface between the air and water. The mechanism of turbulent transfer of momentum and energy in the boundary layer adjacent to the water is somewhat different from that in the layer adjacent to the ground surface. A distinctive feature of the boundary layer over the water is the presence of the moving waves.

There are two characteristics, the first being the wave-driven mean wind. Harris (1966) discovered it in an indoor wave tank. When waves progress in water the waves induce an airflow in the initially still air immediately above the waves with the 'mean component' in the direction of the wave propagation having its velocity maximum at a certain height.

The second characteristic is the perturbed fluctuation of the wind velocity field. The inviscid wave-generation theory was evolved by Miles (1957) and interpreted in physical terms by Lighthill (1962). They considered how a two-

dimensional sheared airflow over water is perturbed by the heaving motions in a harmonic train of waves. Their discussion is based on the concept of a vortex force; when a fluid particle with vorticity moves through a fluid, it will be accelerated at right angles to its direction of propagation.

Laboratory experimentation by Kendall (1970) shows the response of the turbulent flow structure to the perturbations imposed by a wavy wall of smooth neoprene rubber sheet. His result for the mean velocity profile was linear on a semi-log plot. The wall pressure was observed to be asymmetrical about the wave profile, resulting in a pressure drag. The drag was found to be larger than that predicted by the inviscid wave-generation theory and the turbulent structure was strongly modulated by waves.

Recently Davis (1970) investigated two hypotheses concerning turbulent flow over a travelling wave of infinitesimal amplitude. The first turbulent hypothesis is the 'quasi-laminar' assumption (originally introduced by Miles 1957) that the turbulent Reynolds stresses are functions of the height above the mean water level. The second hypothesis (based on Benjamin 1959) is that the properties of the flow are dependent on an appropriate measure of the height above the instantaneous wave surface. Numerical solutions of the equations were compared with Stewart's (1970) experimental results obtained in a wind–wave tunnel and no definite conclusion could be reached from comparison with the experiments, since the predicted flows were quite sensitive to details of the mean velocity profile near the viscous sublayer, where no data were taken.

Measurements of the spectra of fluctuations in wind velocity over the sea were made by Pond, Stewart & Burling (1963), Pond, Smith, Hamblin & Burling (1966) and Weiler & Burling (1967). In all of the cases there was no dominant power spectral peak of the wind turbulence at the dominant frequency of the surface waves. Monotonous distributions in power density were shown in their papers. This is due to the fact that in the atmospheric boundary layer the turbulent fluctuation has much larger energy at about the frequency of the dominant surface waves than the wave-induced wind component.

In the course of experiments on air–sea interaction, we had a very interesting experience on 25 September 1969. When high swells propagated from a typhoon the wind velocity, having a mean value of about 4 m/s and direction opposite to that of the wave propagation, was measured and we found a dominant peak in the spectrum of wind fluctuation at the frequency of the surface waves. The value of this peak was about one order of magnitude larger than the value at neighbouring frequencies, the correlation between surface displacement and wind fluctuation was very high and the phase shift between them was about zero. Recently Yefimov & Sizov (1969) reported a similar observation, but their result for the phase shift between wave and wind fluctuation differs by 180° from our result. In order to explain this discrepancy we have continued the same observation from 1969 to 1970 for different states of the wind and the waves.

The present observations investigate the details of wave-induced wind fluctuation over the sea surface and the present observations are compared with the prediction from the inviscid wave-generation theory.

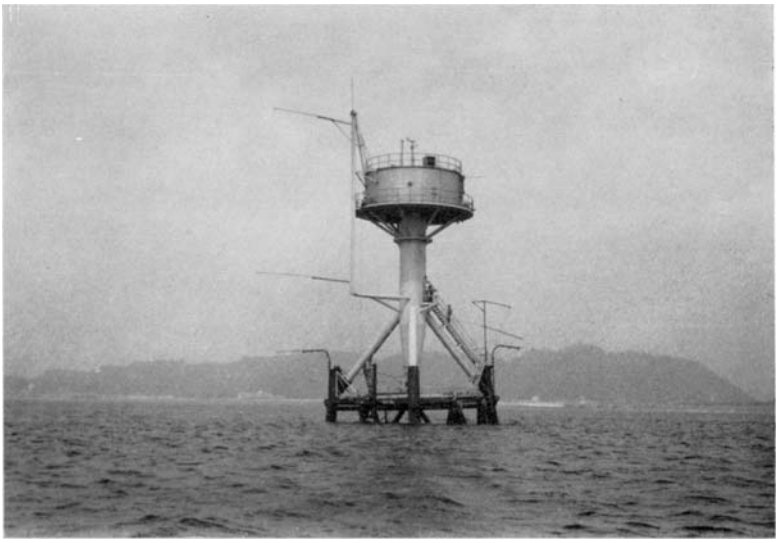

FIGURE 1. Distant view of the Marine Observation Tower.

2. Method of observation

2.1. *Tower*

The observations were made on the Marine Observation Tower of the Institute. A distant view of the tower is presented in figure 1 (plate 1). The location of this tower is near Nijigahama, Hiratsuka City, at a point 1 km distant from the sea shore (lat. 35° 18·1′ N, long. 139° 20·8′ E) in Sagami Bay, which is about 60 km in diameter and faces the Pacific Ocean. The shoreline near this tower extends from west to east. The overall horizontal view is shown in figure 2.

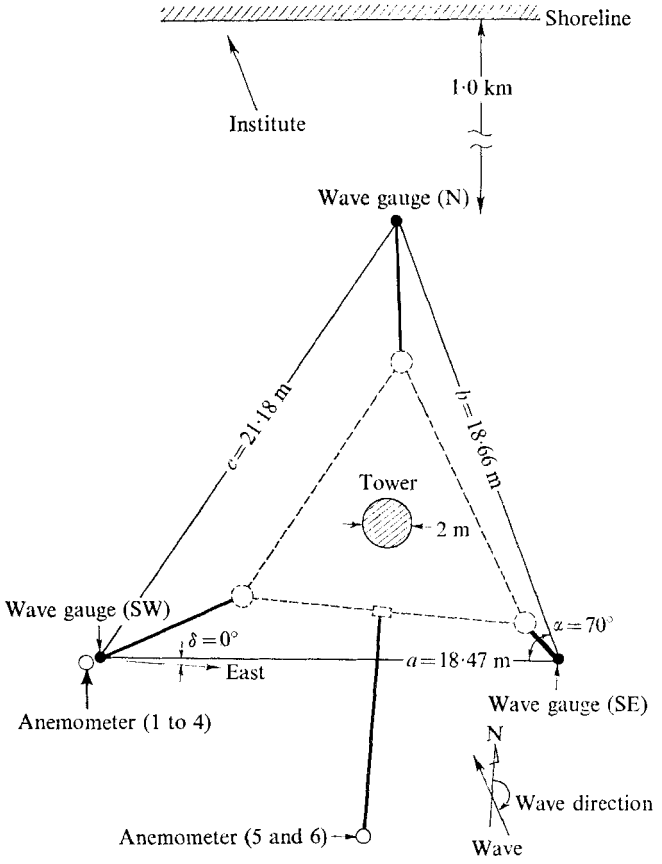

FIGURE 2. Schematic horizontal representation of the marine tower and the positions of the instruments.

The tower proper consists of a tripod of steel-pipe structure erected on the bottom, the water being 20 m deep, a cylindrical structure 2 m in diameter standing 17 m above sea level with a spiral staircase inside, and on top of this a cylinder 3 m high and 7·4 m in diameter containing the observation room. A composite submarine cable consisting of signal wires arranged around three cores of high-voltage power cables was buried in the sea-bed. Outputs of observations by instruments were digitized at the tower, transmitted by a system of bi-phase modulation and processed in the Institute on land with a computer SDS-M92 by an on-line system.

2.2. *Wind velocity*

Measurements of the wind velocity were made by means of six quick-response three-cup anemometers. The light of the lamp was interrupted by a shutter blade connected to a shaft which was turned by the cup assembly. In this way the photocell was illuminated and shaded once for each revolution of the cup assembly. Since the anemometer output was a square pulse form, the period of each revolution was measured through the computer system. Successive revolution rates during one second were analysed. The response time and revolution rate of this anemometer are 0·32 s and about 10 s^{-1}, respectively, when the mean wind velocity is 10 m/s. The other characteristics of the anemometer are described in the paper by Kondo, Naito & Fujinawa (1971).

To avoid an unwanted disturbance of the wind field by the tower, the anemometers are mounted at the end of long horizontal arms. The horizontal distance between the tower centre and the position of the anemometer is 12–13 m. At this distance the error produced by the tower in the measurement of mean wind velocity is 2 or 3 per cent, except in the case where the wind blows in the direction from the tower centre to the anemometer. The disturbed wind field around the tower was determined by direct observation and model testing (Kondo & Naito 1972).

The altitudes of anemometers above the sea surface are about 22 m, 10 m, 5 m, 2·5 m, 1·3 m and 0·8 m, respectively. The upper two anemometers and lower four anemometers are mounted in the directions of south and south-west, respectively, from the centre of the tower. Three horizontal arms supporting the lower three anemometers are joined by vertical struts and are connected to a winch with a wire. When the tide or the wave height becomes high, the lower three anemometers can be pulled up. The mean water level with respect to some fixed level of the tower was sometimes measured by a tide gauge, otherwise we inferred this level from the low-pass filter signal of the capacitance-type wave gauge. Thus, we estimated the distance between the anemometer and the mean water level.

Air temperature and sea surface temperature were measured by means of platinum-wire resistance thermometers. The wind velocity under conditions of nearly neutral stability was analysed in this study.

2.3. *Height, direction and phase velocity of waves*

The elevation of the wave surface and the direction and phase velocity of wave propagation were measured by means of three-capacitance wave-recording gauges, which were supported at the end of horizontal arm in the directions SE, SW and N from the centre of the tower. The sensing element is made of copper wire covered with a vinyl tube 2 mm in diameter. Distances between SW and SE gauges, SE and N gauges, and N and SW gauges are 18·47 m, 18·66 m and 21·18 m, respectively. One of these gauges, the SW gauge, is attached to a point just below the lower four anemometers.

After the calculation of the coherence and the phase shift ϕ between output voltages of the wave gauge system has been made, the direction and phase

velocity of wave for each frequency component can be estimated. The wave direction θ is expressed in the equations (see figure 2)

$$\theta = -\delta + \tan^{-1}(\sin\alpha/(\cos\alpha - a\phi_2/b\phi_1)) \quad (\phi_1 \geqslant 0), \tag{1}$$

$$\theta = \pi - \delta + \tan^{-1}(\sin\alpha/(\cos\alpha - a\phi_2/b\phi_1)) \quad (\phi_1 < 0), \tag{2}$$

where ϕ_1 and ϕ_2 are the phase shifts between the SE and SW wave gauge output voltages and between the SE and N wave gauge output voltages, respectively. The positive ϕ indicates that the output voltage of the SE wave gauge leads the other ones. The wavelength λ and the phase velocity of wave propagation C are expressed as

$$\lambda = 2\pi l_1/\phi_1 = 2\pi l_2/\phi_2, \tag{3}$$

$$\lambda = C/f, \tag{4}$$

where f is the frequency and

$$l_1 = a\sin(\theta+\delta), \quad l_2 = b\sin(\theta+\delta-\alpha). \tag{5), (6}$$

The phase velocity of wave propagation as a function of frequency is observed to be roughly the same as the theoretical relation (equations (10) and (11) below) accompanied by some scattering.

3. Vertical profile of the mean wind velocity

Many experimental results show that the vertical profile of the mean wind velocity in the layer adjacent to the water is close to logarithmic, if thermal stratification is absent. Logarithmic profiles are shown by Roll (1965) above the sea surface, and by Shemdin & Hsu (1966), Kato & Takemura (1966) and Wu (1968) for an indoor wave tank. Stewart's (1970) profile, over waves in a wind–wave tunnel, is the same as that over a rough plate; the mean velocity varies as the logarithm of the height above the mean water level, except very close to the water surface, where the effect of the molecular viscosity becomes important. However, some results differing from logarithmic profile have been reported by Takeda (1963) over shore waves, by Hamada (1968) for an indoor wave tank, by Nan'niti, Fujiki & Akamatsu (1968) and by Yefimov & Sizov (1969) over the sea. These all show a kink in the profile just above the wave surface.

During the present observations the mean wind profile below the level of 6 m received special attention, with wind velocities of 3–7 m/s and wave heights of 70–100 cm. As the arms of the lower three anemometers are joined with vertical struts and connected to a winch, their altitude can be easily increased or decreased. An example of the profile of mean wind velocity, during a period of 10 min, is shown in figure 3. This was obtained immediately after the calibration had been made. The ratio of the mean wind velocity to the wind velocity at a height of 6 m is shown as the abscissa, the vertical co-ordinate being the distance from the mean water level. The scale of the abscissa for the leftmost profile is shown. The scales for other profiles are shifted to the right in steps of 0·05. Numbers attached to the lines indicate the observation time. Directions of the

wind and the wave propagation were both south. The mean wind velocity was about 300–400 cm/s and the maximum height of the swelling waves about 70 cm.

We can see the straight line profile in the logarithmic height co-ordinate, without any appreciable kink character. Such a logarithmic profile is also reported by Kendall (1970) above a wavy wall which is mechanically deformed at controlled speed.

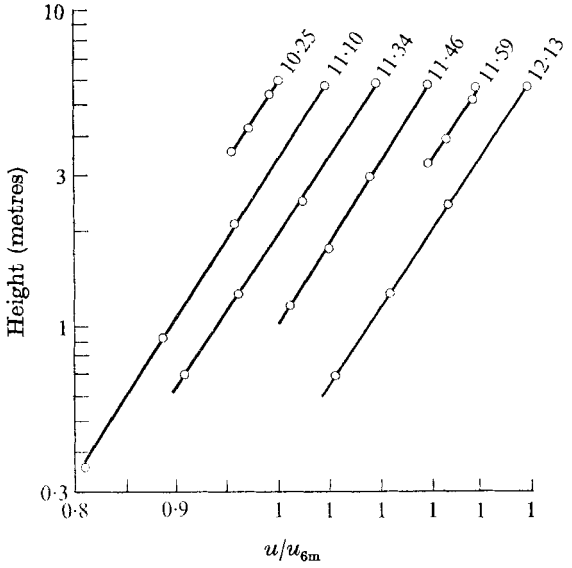

FIGURE 3. Successively measured vertical profiles of mean wind velocity (3 July 1970) with u/u_{6m} shown as abscissa. The relative wind scale for leftmost profile is shown and the other profiles are shifted to the right at intervals of 0·05.

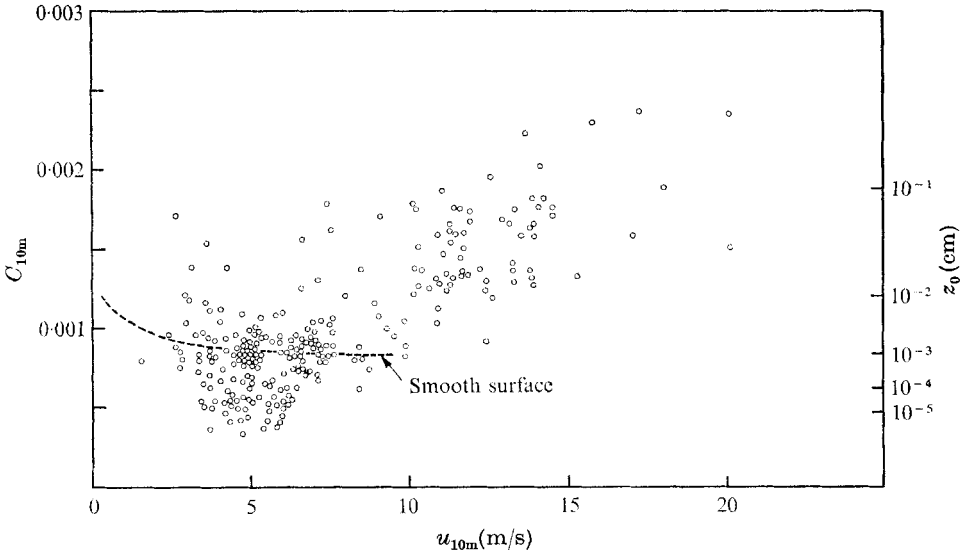

FIGURE 4. Drag coefficient C_{10m} of the sea surface as a function of wind velocity at a height of 10 m, u_{10m}, under conditions of nearly neutral stability. The aerodynamical roughness height z_0 is shown on the ordinate at the right-hand side.

From a much larger series of observations the friction velocity u^* and the drag coefficient at a height of 10 m, $C_{10m} = (u^*/u_{10m})^2$, were calculated. Figure 4 shows the drag coefficient as a function of wind velocity at a height of 10 m, u_{10m}, under conditions of nearly neutral stability. The relation is obtained from observations in the layer below 22 m. Wind velocity at the common 10 m level is obtained from the present data by assuming a logarithmic wind law. When $u_{10m} < 7$ m/s the drag coefficient lies around the curve for aerodynamically smooth flow (broken line), while when $u_{10m} > 7$ m/s it is increased with wind velocity.

For comparison with the present results, we may consider the recent findings of Hicks & Dyer (1970), who also found little variation in drag coefficient with wind velocity below 9 m/s, an average value of 0·001 being obtained. Deacon & Webb (1962) found a value 0·001 in case of light wind, increasing to about 0·002 at the wind velocity of 14 m/s. Phillips (1966) obtained values from 0·001 to 0·002. Each of these findings is very close to the present result.

4. Correlation between the sea surface displacement and the horizontal component of the wind velocity

Cases of nearly neutral stability (see Lumley & Panofsky 1964) are analysed in this paper. The sampling periods of observation are 25 min for all runs, except for run 10 when the period was 10 min. Figure 5 shows 100 s sections of wave and wind records. The dotted line is the wave record, the solid lines are the wind velocity fluctuations at different heights. Numbers on the solid lines indicate the anemometer heights z above the mean water level. The upper part of this figure, run 61 (on 18 June 1970), shows the case where the air and wave move roughly in the same direction: the wind direction being 190° from north and the swell direction 145° from north. Negative correlation between the surface displacement and the wind velocity can be clearly seen in the lower three traces of the wind at $z = 0{\cdot}8$ m, 1·37 m and 2·6 m. The lower part of figure 5, run 10 (on 25 September 1969), shows another case where the air and wave move in opposite directions. In this case the swelling wave with a period of about 12 s comes from the south and the light wind blows from north–north-west. A periodic fluctuation of about period 12 s can be seen in the wind record at every level.

An essential difference between the upper figure and the lower one is seen in the phase shift between the sea surface displacement and the wind fluctuation. This is about 180° in the upper figure; the fast wind occurs above the trough of wave and the slow one above the ridge of wave. On the other hand, in the lower part of figure 5 a phase shift of about zero is shown. (The delay time of the cup anemometer due to the mechanical inertia is about 1 s for these cases. This will be corrected in a later section.) The wind blows faster above the ridge and slower above the trough.

Typical examples of cross-correlation coefficients between the sea surface displacement and the wind velocity are shown in figure 6. A positive time lag indicates that the sea surface displacement leads the wind velocity, a negative time lag that the sea surface displacement lags behind the wind velocity. A

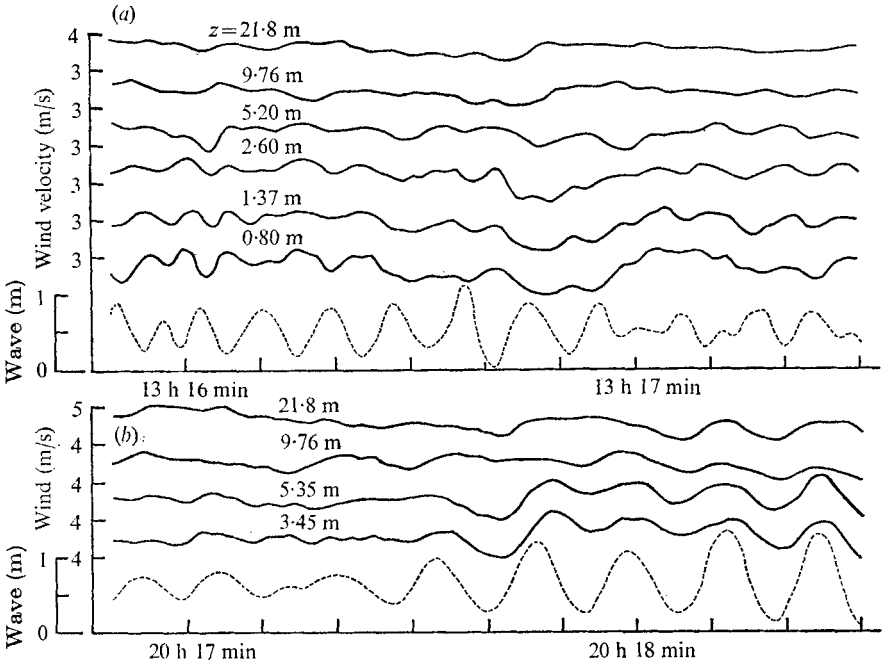

FIGURE 5. Smoothed traces of wave records (dotted line) and wind records (solid lines). The scale of wind velocity observed by the top anemometer is shown and the others are shifted to downward at intervals of 1 m/s. (*a*) Run 61 (18 June 1970), air and the wave move in the same direction. (*b*) Run 10 (25 September 1969), the case of adverse direction.

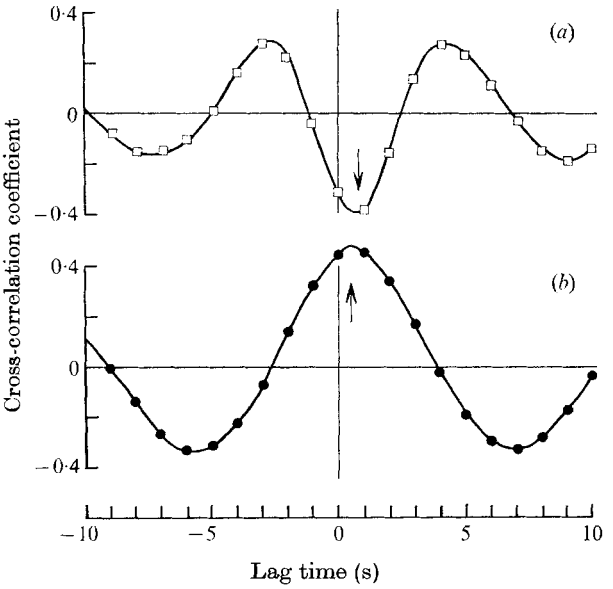

FIGURE 6. Examples of cross-correlation coefficients between the sea surface displacement and the wind velocity. Positive lag indicates that the surface elevation leads the wind velocity and negative lag indicates that the surface elevation lags behind the wind velocity. (*a*) Run 61, z = 260 cm, (*b*) Run 10, z = 345 cm.

curve for the co-current case (run 61) is shown on the upper part of this figure and the anti-current case (run 10) on the lower part. The two curves in figure 6 are the cases with light winds of 317 cm/s (run 61) and 383 cm/s (run 10). In general, the correlation coefficient decreases with increasing wind velocity and distance from the sea surface.

The arrow in figure 6 shows the position where the cross-correlation coefficient takes the maximum absolute value. One of the reasons for this positive lag is the inertia of the cup anemometer. A delay time due to the mechanical inertia is given by Kondo, Naito & Fujinawa (1971). The correction to the time lag will be made in a later section.

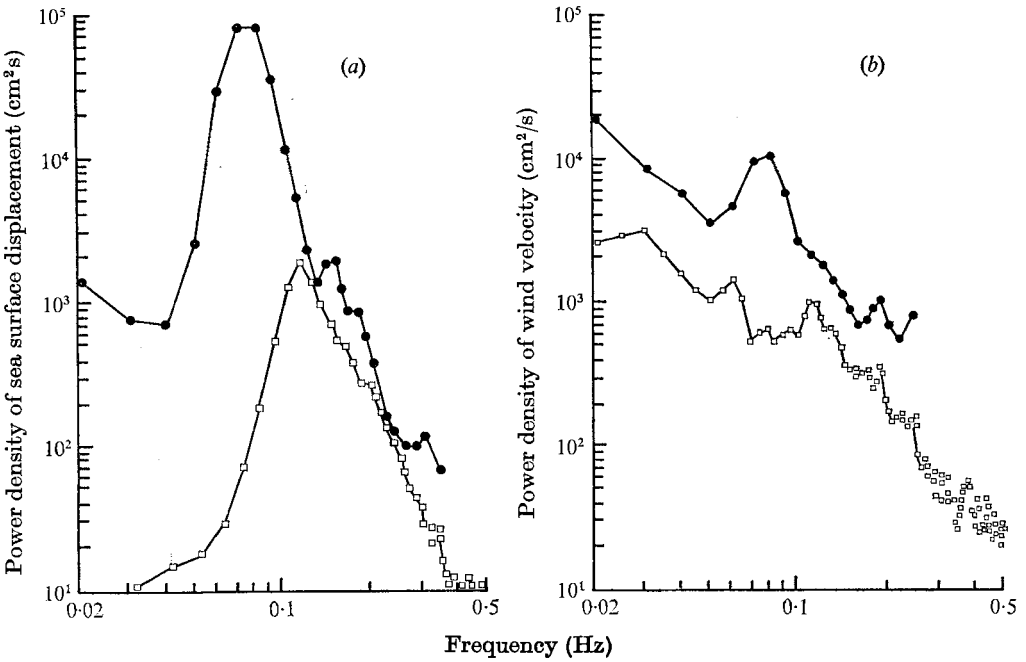

FIGURE 7. Power spectra of (*a*) sea surface displacement, (*b*) wind velocity fluctuation. □, run 61, $z = 260$ cm, $u = 317$ cm/s; ●, run 10, $z = 345$ cm, $u = 383$ cm/s.

The power spectra of the sea surface displacement and wind velocity fluctuations for runs 61 and 10 are presented in figure 7. A peak in power density of the sea surface displacement can be seen at a frequency of 0·12 Hz for run 61 and at 0·08 Hz for run 10. As for the power density of wind fluctuation, a dominant value can be seen near the frequency at which the energy of sea surface displacement takes its peak value.

Figure 8 shows the spectral characteristics of the correlation between the sea surface displacement and the wind velocity fluctuations at different levels. The square root of coherence is considered to be the correlation coefficient for each frequency. Higher values of coherence are shown in the frequency range where the energy of sea surface displacement has its peak value. The coherence is larger at the frequency range from 0·1 to 0·2 Hz for run 61 and from 0·06 to 0·18 Hz for run 10.

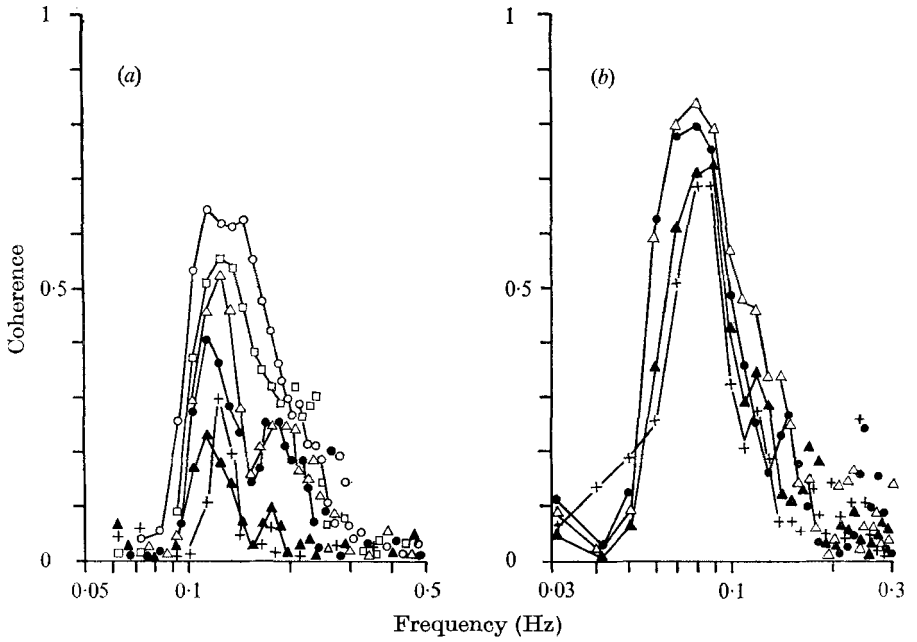

FIGURE 8. Coherences between the surface displacement and the wind velocity at different levels. +, $z = 2181$ cm: ▲, $z = 976$. (*a*) Run 61: ●, $z = 520$ cm; △, $z = 260$; □, $z \simeq 139$; ○, $z = 80$. (*b*) Run 10: ●, $z = 535$ cm; △, $z = 345$.

5. Phase shift between the sea surface displacement and the wind fluctuations

As is shown in figures 5 and 6 the phase shift between the sea surface displacement and the horizontal component of wind fluctuation depends on the relative velocity between the mean wind velocity and the phase velocity of wave propagation, and, as mentioned above, it also depends on the response characteristics of the anemometer. Corrections to original observations of phase shift due to the latter cause were made by use of a result by Kondo *et al.* (1971). When the wind has the mean velocity of 10 m/s with a frequency of 0·1 Hz (period of 10 s), for example, the delay time due to inertia of the present anemometer is about 0·32 s (0·2 radian = 12 degrees). As another example, when the wind has a frequency of 0·2 Hz (period of 5 s) and mean velocity of 5 m/s the delay time is 0·56 s (0·7 radian = 40 degrees). The phase shift in each frequency component is defined as the tangent of the ratio of imaginary to real parts in the cross-spectrum between the sea surface displacement and the wind velocity (see equation (7)).

Observations are divided into three groups according to the relative velocity between the mean wind velocity u and the phase velocity of wave propagation C: (i) Case of $(u - C) < 0$, at low wind velocity and with swell. (ii) Case of $u > 0 > C$, when the air and wave move in opposite directions. (iii) Case of $u \simeq C$, near the critical level where the air velocity equals the wave phase velocity.

5.1. *Case of* $(u-C) < 0$

An example of the phase shift between the sea surface displacement and the wind velocity fluctuation is shown on the left of figure 9. The lag of the Fourier component of the wind velocity behind the sea surface displacement component for the frequency range of 0·1–0·25 Hz is 150–185°. A much larger series of

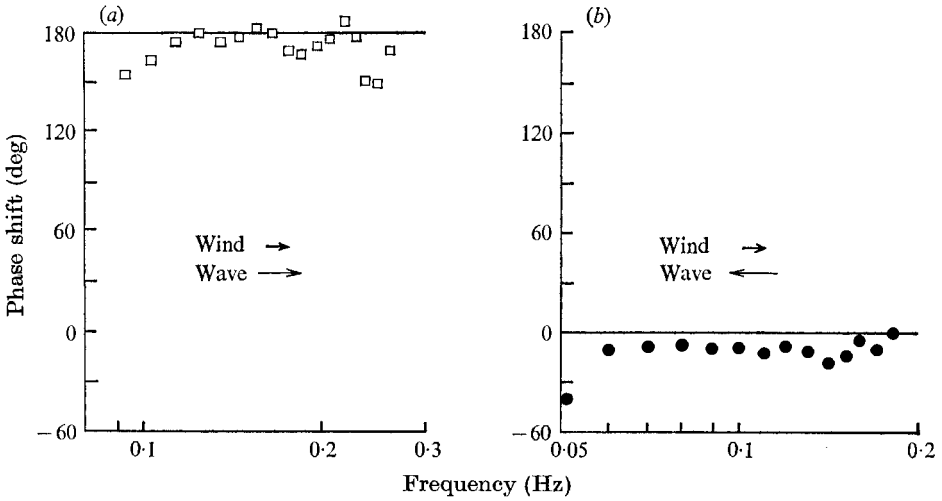

FIGURE 9. Phase shift between the sea surface displacement and the wave-induced wind velocity. Positive value designates that the surface displacement leads the wind velocity. (*a*) Run 61, $z = 260$ cm, favourable wind case. (*b*) Run 10, $z = 345$ cm, adverse wind case.

observations shows that the phase shift for the frequency range where the value of the spectral density of the sea-surface displacement is large is about 160–190°.

5.2. *Case of* $u > 0 > C$

An example for run 10 is shown on the right of figure 9. The phase shift for the frequency range of 0·06–0·18 Hz is about −20–0°. The data other than those of this example show the phase shift to be −20–10°. This means that the velocity for each frequency component becomes high above the ridge of wave and low above the trough of wave. Almost the same result was shown in a wind tunnel experiment by Kendall (1970). His result shows that the pressure distribution is shifted by about 0–10° downwind with respect to the surface depression profile of a wavy wall with a smooth neoprene rubber sheet when air and wave move in opposite directions ($C/u = -0{\cdot}5$–0).

5.3. *Case of* $u \simeq C$

With this condition the correlation between the surface displacement and the wind velocity fluctuation becomes very low and the phase shift becomes obscure. Therefore, after the average values of the real and imaginary parts in the cross spectra between the sea surface displacement and the wind velocity over several successive observation runs have been calculated we obtain the vector means

over some frequency ranges of the phase shift and of the amplitude ratio of the wave-induced wind velocity fluctuation to the sea surface displacement. This enables one to detect the very weak wave-induced wind component in the presence of relatively high amplitude turbulence.

An example is displayed in figure 10. This is the mean of runs 82–84 (11–12 July 1970). The lag of each frequency component of the wind velocity behind the sea surface displacement component for frequencies of 0·1–0·25 Hz is about 180° but it changes abruptly at a frequency of 0·25 Hz, taking a negative phase shift for frequencies of 0·25–0·45 Hz. The solid line shows the predictions from the inviscid calculations of Conte & Miles (1959) which will be briefly surveyed in § 7.

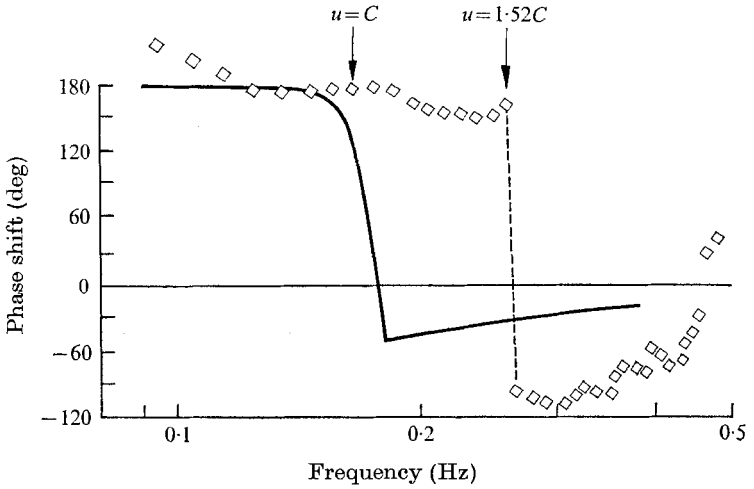

FIGURE 10. Same as figure 9 but for the mean of runs 82, 83 and 84. $z = 239$ cm, $u = 911$ cm/s.

Direct comparison between theory and the present observations cannot be done simply, because the theoretical relation is expressed in terms of η, the height from the instantaneous wave surface, but our observations are referred to the spatially fixed point z, the vertical distance from the mean water level. However, some calculations show that in the layer far from the wave surface, as in the present observations, the difference between the observed value of wave-induced wind fluctuation in terms of η and that in terms of z is relatively small in comparison with the difference between the theoretical value in terms of η and the observed one in terms of z. Some examples comparing the wave-induced wind in terms of η with that in terms of z will be shown later.

In a rough comparison between the inviscid theory and the present observation, some discrepancies can be seen in figure 10. The phase reversal frequency is lower in the theory than in the observation. The ratio of the phase reversal frequency from theory and that from observation is about 1·5 for this example. In all cases the abrupt change in phase shift occurs at a higher frequency than is predicted by the theory and, in general, the difference between these frequencies increases with the height above the mean water level. In other words, if we consider one frequency component, the phase shift between the sea surface displacement and the wind velocity fluctuation is about 180° at the layer adjacent

to the water surface where the wave velocity C overtakes the mean wind velocity u and also at the critical height z_c, where the wave velocity equals the mean wind velocity, and the phase shift is abruptly reversed to the negative value at the height where $u = 1{\cdot}2C$–$1{\cdot}5C$. This height, for example, may be estimated to be about 6–100 m if $C = 10$ m/s, $z_c = 1$ m and the aerodynamic roughness height $z_0 = 0{\cdot}01$ cm.

The height of the phase reversal point has been obtained in indoor experiments of Shemdin & Hsu (1966), Gupta, Landahl & Mollo-Christensen (1968), Hussain & Reynolds (1970), Kendall (1970) and Stewart (1970). Shemdin & Hsu's experiment (1966, figures 21 and 45 and table 3) for pressure distribution over mechanically generated water shows that when the pressure sensor is fixed in space 0·5 in above the crest of a wave 3 in. high the pressure distribution is out of phase with the wave (that is, wind velocity fluctuation is in phase with wave) for the case of $u = 0$. The experiment also shows that the pressure signal becomes minimum in amplitude when $u \simeq C$ and is shifted by 75° with respect to the wave when $u \simeq 1{\cdot}5C$ and that the pressure trace is 180° out of phase (that is, the wind velocity is in phase) with respect to the wave when the pressure sensor remains far above the critical layer. Kendall's wind tunnel experiment (1970, figure 8(*b*)) shows that below the critical height the wind fluctuation, which is induced by wavy wall with a neoprene rubber sheet, is 180° out of phase with respect to the wave and that at $u > 2{\cdot}0C$ a phase reversal can be seen.

6. Ratio of the amplitude of the wave-induced wind fluctuation to that of the sea surface displacement

The cross-spectrum between the sea surface displacement η and the wind velocity u is expressed by (see Lumley & Panofsky 1964)

$$\phi_{\eta u} = C_{\eta u} - iQ_{\eta u}. \tag{7}$$

$C_{\eta u}$ is called the co-spectrum and $Q_{\eta u}$ the quadrature spectrum (or the real and the imaginary parts of the cross-spectrum, respectively). The amplitude ratio of the sea surface displacement to the wave-induced wind velocity is calculated from

$$(\text{Amplitude ratio})^2 = (C_{\eta u}/P_\eta)^2 + (Q_{\eta u}/P_\eta)^2, \tag{8}$$

where P_η is the power density of the sea surface displacement.

The amplitude ratios at different heights for each run were calculated. An example of the case of $u \simeq C$ is presented in figure 11. In this case the wave-induced wind component is very weak as compared with the turbulent wind component so the vector mean over successive observation runs is presented. The amplitude ratio takes its minimum value at frequencies from 0·23–0·29 Hz and its frequency corresponds with the phase reversal point. The calculated result from the inviscid theory of Conte & Miles (1959) (see § 7) is shown as a solid line. Some discrepancies between the theory and the observation can be found. The observed frequency where the amplitude ratio takes a minimum value is larger than the theoretical one, as is shown in the phase reversal frequency, and in general at the highest

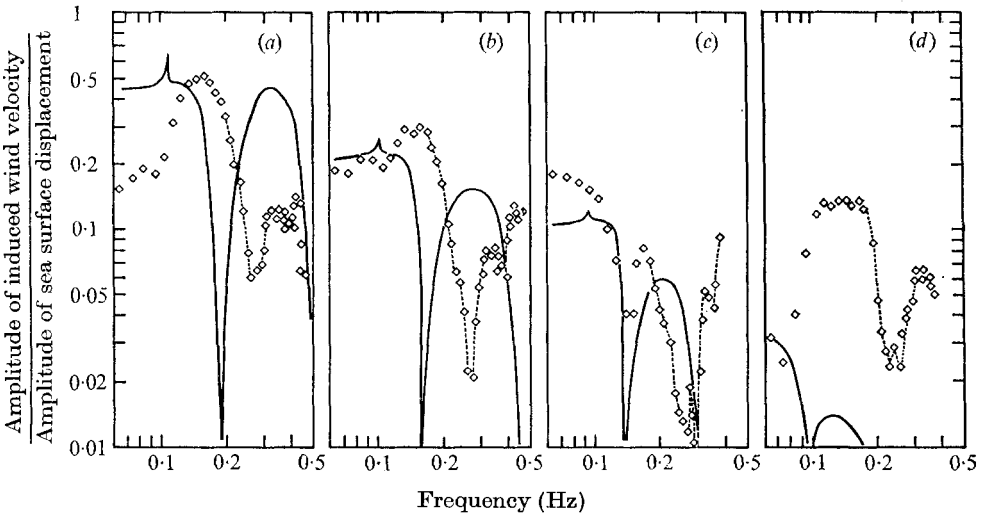

FIGURE 11. Ratio of the amplitude of the wave-induced wind velocity to that of the sea surface displacement for the mean of runs 82, 83 and 84. (*a*) $z = 239$ cm; (*b*) $z = 493$; (*c*) $z = 949$; (*d*) $z = 2154$; ——, prediction from the inviscid theory.

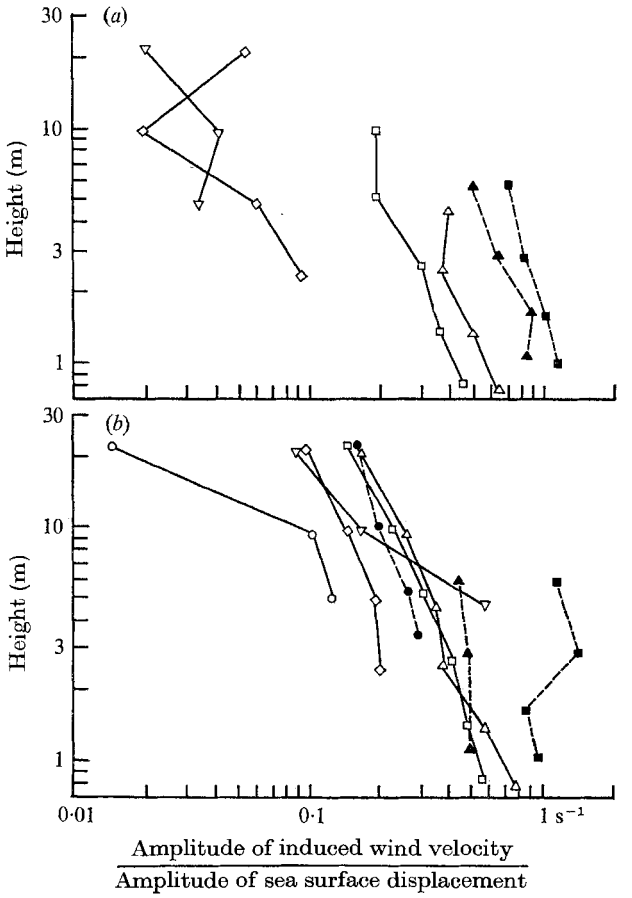

FIGURE 12. Height dependency of magnitude of (*a*) 0·1 Hz and (*b*) 0·3 Hz frequency components of the wave-induced wind velocity. The open symbols express the favourable wind cases and the blocked ones the adverse wind cases. □, runs 60–63, $u^* = 8$ cm/s; △, runs 64–68, $u^* = 14$; ◇, runs 82–84, $u^* = 44$; ▽, runs 92–107, $u^* = 49$; ○, runs 42–59, $u^* = 54$; ●, run 10, $u^* = 14$; ■, runs 69–71, $u^* = 15$; ▲, run 72, $u^* = 17$.

level the observed value of the amplitude ratio is large as compared with the theoretical one, especially at higher frequency.

Figure 12 shows the height dependency of the amplitude ratio. The mean frequency values of about 0·1 Hz (the lower part) and of 0·3 Hz (the upper part) for each series are plotted in the figure. The white symbols indicate the favourable wind case and the black ones the adverse wind case. For the lower frequency (0·1 Hz, see figure 12) the decrease of the amplitude ratio with height is not so sharp and is in accord with the inviscid theory, at least qualitatively. However for higher frequencies (see also figure 11) the decrease of the observed amplitude ratio is considerably smaller than that predicted from the inviscid theory. This difference can be partly attributed to the fact that z is used as a co-ordinate for the observations and η is used for the theory (see figure 13) but a full explanation cannot be given.

7. Calculation according to the theory of inviscid fluids

If we denote the wave-induced perturbation stream function as $\Phi(z)\,e^{ikx}$, then Φ satisfies the inviscid Orr–Sommerfeld equation

$$(u-C)(\Phi''-k^2\Phi)-u''\Phi=0, \tag{9}$$

in the inviscid turbulent-stress discard approximation, where a prime denotes differentiation with respect to the vertical co-ordinate z, k denotes the wave-number and x the horizontal co-ordinate in the direction of wave propagation (Phillips 1966).

The procedure for numerical integration of this equation has been given by Conte & Miles (1959) and we followed their method in the theoretical computation of the magnitude and phase of wave induced perturbation velocity. In practical calculation we used the following theoretical relationship between wave frequency f and phase velocity of wave C for water of depth $d = 20$ m (Lamb 1945, p. 738):

$$C^2=(g\lambda/2\pi)\tanh(2\pi d/\lambda)+2\pi T/\rho\lambda, \tag{10}$$

$$C=f\lambda, \tag{11}$$

where λ is the wavelength, g the acceleration due to gravity, ρ the density of water and T the surface tension of water. The effect of surface tension as expressed by the second term on the right of the equation is usually much smaller than the first term and has in general been neglected.

It can easily be seen from order estimation or direct comparison with exact numerical calculation that the approximate solution

$$\Phi=A(u-C)\,e^{-kz}, \tag{12}$$

where A is the amplitude of the wave component, given by Miles (1957) and Lighthill (1957), is a fairly good approximation below the critical layer, so we used this solution when wind velocity was weak and C/u^*, where u^* is the friction velocity, exceeded 15.

Now, as asserted by Miles (1957) and Benjamin (1959), the argument of Φ must be considered to be η, the co-ordinate normal to the water surface such that $\eta = 0$ becomes the water surface, rather than the vertical distance z from the mean water level and we cannot simply compare the observed and theoretical results, as our observations were referred to the spatially fixed point. Let us estimate the difference between $\Phi(\eta)$ and $\Phi(z)$. The transformation is given by Benjamin (1959) as

$$\eta = z - A\, e^{-kz} \cos kx. \tag{13}$$

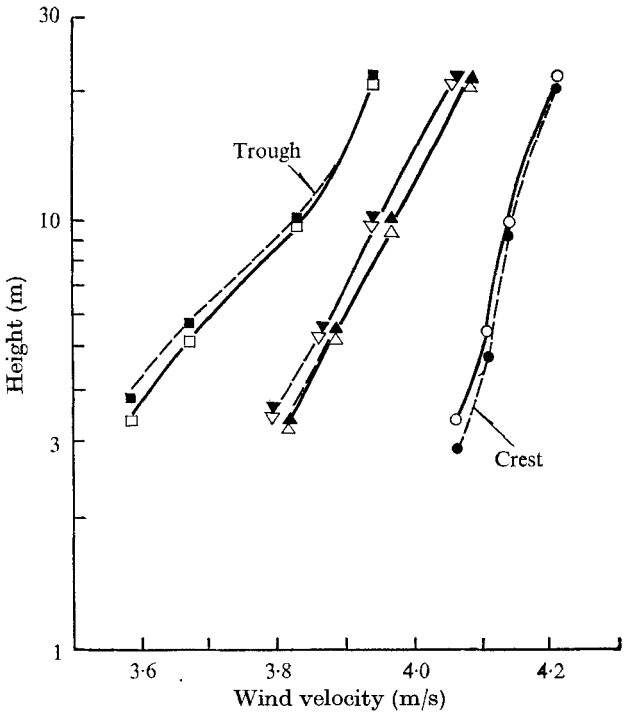

FIGURE 13. Instantaneous wind velocity distribution over four points of wave surface for run 10. ○, ●, crest; □, ■, trough; △, ▲, ½ wavelength distance from the crest; ▽, ▼, ¾ wavelength distance from the crest. Height is measured from the mean water level (z co-ordinate) for the solid line and the open symbols, and from the instantaneous wave surface (η co-ordinate) for the broken line and the blocked symbols.

Thus $\Phi(\eta)$ can be expressed by the spatial function as

$$\Phi(\eta) = \Phi(z - A\, e^{-kz} \cos kx). \tag{14}$$

As the wave amplitude is infinitesimal, we can expand this as

$$\Phi(\eta) = \Phi(z) + \Phi'(z)\,(-A\, e^{-kz} \cos kx) + \tfrac{1}{2}\Phi''(z)\,(A^2 e^{-2kz} \cos^2 kx) + \ldots, \tag{15}$$

if Φ varies moderately. Taking the mean over a wavelength we get

$$\overline{\Phi(\eta)} = \Phi(z) + O(A^2). \tag{16}$$

The difference is of the second order in wave amplitude and is negligible.

In other words, it can be said that when the observational level is far distant from the wave surface as compared with the amplitude of the sea surface displacement, the observed amplitude of wave-induced wind at a spatially fixed point is nearly the same as that observed at an ideal buoy which follows the instantaneous sea surface. An example of the difference between the instantaneous wind profiles over wave surface expressed in terms of the z and that in terms of η is shown in figure 13 (run 10). In run 10 the mean and the root-mean-square values of the wave height are 90 and 38 cm, respectively. The figure shows the case in which the phase shift between the sea surface displacement and the wave-induced wind velocity is nearly zero. It can be seen from the figure that the amplitude of wind velocity at a height of 3 m, in terms of z, is smaller by 8 per cent than that in terms of η. On the other hand in the case of a phase difference of 180° between the sea surface displacement and wind (not presented in this figure) the amplitude of wave-induced wind velocity as observed in terms of z becomes larger than that in terms of η by several per cent.

8. Wave form

In run 10 the sea surface displacement with a frequency of 0·08 Hz (period 12·6 s) is picked out. Data during 10 min of the sea surface displacement and the wind velocity are cut into 48 pieces at each of the crests of the sea surface displacement. Arranging each piece of a 12 s section in 48 lines and obtaining an average over one period, a wave form from the crest to the crest of the sea surface displacement is obtained and such a wave form for the wind velocity is obtained similarly. A wave form from trough to trough is obtained by the same method. In this way the wave forms of the sea surface displacement and the wind velocity are displayed in figure 14. The dot–dash line is a sine curve and the lower part of this figure, a line with the crosses, is the wave form of the surface wave. The upper four lines are the wave forms of the wind fluctuations at z = 345, 535, 976 and 2181 cm. The ordinate for the top line is shown and the other is shifted downward in steps of 10 cm/s. Small distortions of the wave form from the sine curve can be seen in the figure. These are partly due to different delay characteristics in accelerating and decelerating conditions of the cup anemometer (Kondo *et al.* 1971), partly to the distorted form of the sea surface displacement and partly to the nature of the wave-induced wind. Nevertheless, the distortion of the wave form of the wind velocity from that of the surface displacement is relatively small, at least at the lower frequency range of the present observation.

Indoor experiments of Shemdin & Hsu (1966) and Kendall (1970) show a large distortion in the wave form of the wind velocity fluctuation. This asymmetrical form of the wave profile results in a pressure drag. Their indoor experiments were made for a shorter wavelength; Kendall had λ = 4 in. From our small distortion for longer waves over the sea and their large distortion for shorter waves indoors it may be inferred that the average pressure drag of sea surface is partly due to the contribution of the higher frequency component of the waves.

9. Discussion

The findings from the present observations of the longitudinal component of wave-induced wind fluctuation are that there exists a component 160–190° out of phase with respect to the wave in the layer adjacent to the sea surface where the wave phase velocity overtakes the wind and that above this layer a phase reversal takes place and the phase shift between the wave and the wind takes some negative value. When the air and wave move in opposite directions the wave-induced wind is found to be in phase with respect to the sea surface displacement.

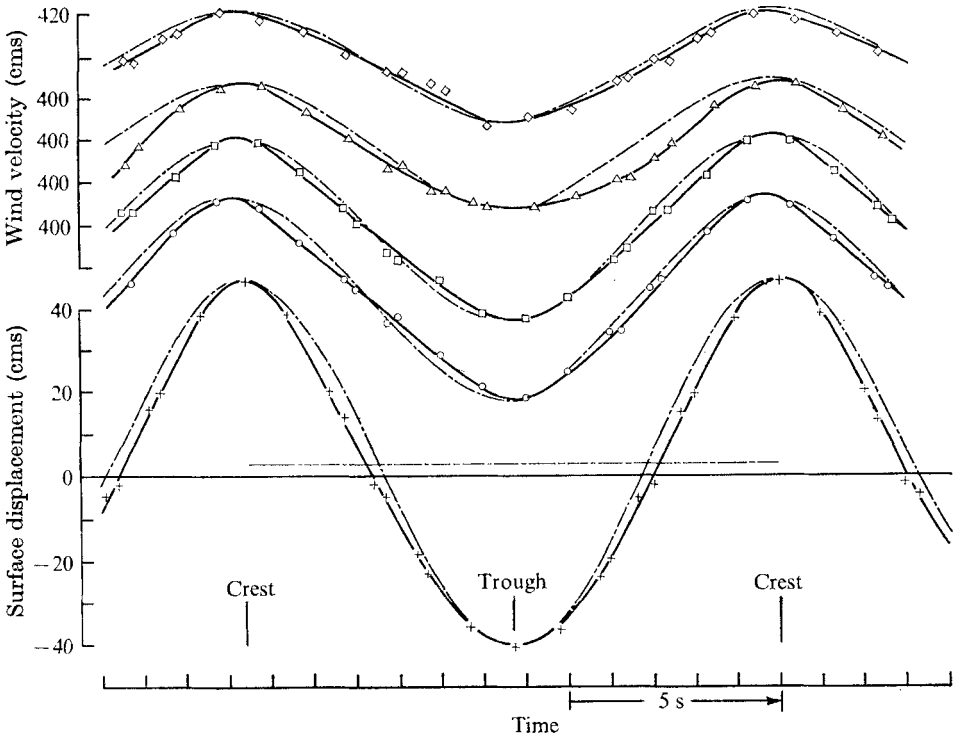

FIGURE 14. The wave forms of the wave-induced wind at different levels and that of the sea surface displacement for run 10 (25 September 1969). Wave-induced wind: —◇—, $z = 21{\cdot}8$ m; —△—, $z = 9{\cdot}76$; —□—, $z = 5{\cdot}35$; —○—, $z = 3{\cdot}45$. —+—, sea surface displacement; — · —, sine curves for reference. The ordinate of wind velocity for top line is shown and the other is shifted downward in steps of 10 cm/s.

Naturally, the mechanism of turbulent transfer in the boundary layer adjacent to the sea surface cannot be definitely obtained from only these findings, but they will certainly throw a fresh light on the future course of the study on the turbulent transfer mechanism over the sea.

Some discrepancies between the present observations and inviscid theory are presented. It may be considered that the cause of the discrepancy is partly the turbulent diffusion, which is not taken into account in the theory, partly the three-dimensional pattern of the sea surface and partly the interaction between different frequency components. Some indications of this are shown in figures 15

and 16. Figure 15 shows the coherence between the sea surface displacements at two points separated by a distance $a = 18{\cdot}47$ m (see figure 2) in figure 15(*a*) and by $b = 18{\cdot}66$ m in figure 15(*b*). The coherence is expressed as a function of the

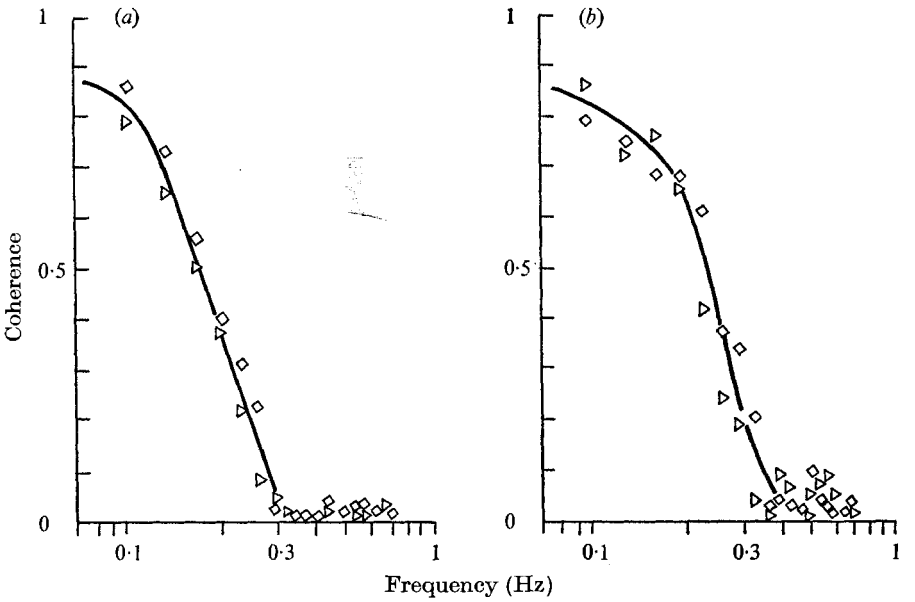

FIGURE 15. Examples of the coherence between (*a*) the output of SE-wave gauge and that of the SW-wave gauge and (*b*) the SE-wave gauge and N-wave gauge; ◇, run 82; △, run 84.

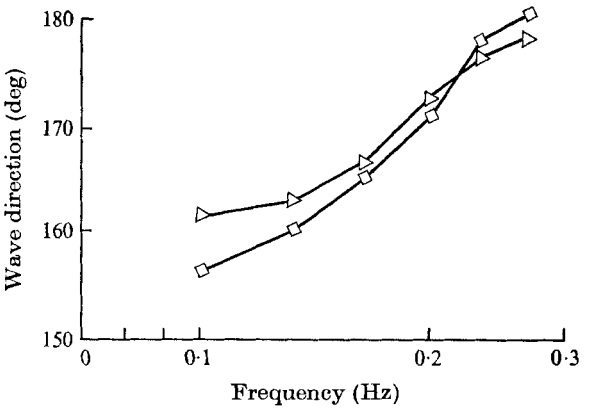

FIGURE 16. Examples of the wave direction as the function of frequency. ◇, run 82; △, run 84.

frequency. The coherence in the frequency range above 0·3–0·4 Hz is very small; this corresponds to wavelengths shorter than 17–10 m. In other words, the wind wave does not have the characteristics of motions in an infinite harmonic train of waves. A wave has been formed and propagates over a certain distance, almost preserving its wave property; thereafter the original wave form is deformed and then vanishes. This may be attributed to the fact that the sea wave has two-

dimensional and dispersion characteristics and that the higher frequency components of waves decay by the action of the turbulence in the water.

In most cases on the sea surface, the direction of propagation of the wind waves, which come to a site of observation from nearly the same direction as the wind, is different from that of the swell which has a low frequency component and comes from a distant place. Figure 16 shows two examples of the wave direction as a function of frequency. The wave with a lower frequency component, the swell, comes from south–south–east but the direction of wave propagation is shifted southwards as the wave frequency increases. Most experiments in an indoor wave tank have hitherto been made for the case where an inflow of air over the wave surface is of relatively low intensity of turbulence. In contrast with this there is high intensity of turbulence in the atmospheric boundary layer.

The authors are particularly indebted to Professor Giichi Yamamoto of Tohoku University, Sendai, and Dr Kazuhiko Terada, Director of National Research Center for Disaster Prevention, Tokyo, for encouragement during the course of this research. Thanks are also extended to Dr Noriyuki Iwata for valuable comments and to Mr Isao Watabe for his assistance in this study. The partial financial support of the Ministry of Education under a Grant in Aid for Fundamental Scientific Research and that of the Japan Society for the Promotion of Science are gratefully acknowledged.

REFERENCES

BENJAMIN, T. B. 1959 Shearing flow over a wavy boundary. *J. Fluid Mech.* **6**, 161–205.

CONTE, S. D. & MILES, J. W. 1959 On the numerical integration of the Orr–Sommerfeld equation. *J. Soc. Industr. Appl. Math.* **7** (4), 361–366.

DAVIS, R. E. 1970 On the turbulent flow over a wavy boundary. *J. Fluid Mech.* **42**, 721–731.

DEACON, E. L. & WEBB, E. K. 1962 Interchange of properties between sea and air. Chapter 3. Small-scale interactions. In *The Sea* (ed. M. N. Hill), p. 43. Interscience.

GUPTA, A. K., LANDAHL, M. T. & MOLLO-CHRISTENSEN, E. L. 1968 Experimental and theoretical investigation of the stability of air flow over a water surface. *J. Fluid Mech.* **33**, 673–691.

HAMADA, T. 1968 On some properties of wind over water waves (with English abstract). *Rep. Port & Harbour Tech. Res. Inst.* **7** (4), 22.

HARRIS, D. L. 1966 The wave-driven wind. *J. Atmos. Sci.* **23**, 688–693.

HICKS, B. B. & DYER, A. J. 1970 Measurements of eddy-fluxes over the sea from an offshore oil rig. *Quart. J. Roy. Meteor. Soc.* **96**, 523–528.

HUSSAIN, A. K. M. F. & REYNOLDS, W. C. 1970 The mechanics of an organized wave in turbulent shear flow. *J. Fluid Mech.* **41**, 241–258.

KATO, H. & TAKEMURA, K. 1966 Wind profiles over the shallow water (1st report, with English abstract). *Rep. Port & Harbour Tech. Res. Inst.* **5** (1), 26.

KENDALL, J. M. 1970 The turbulent boundary layer over a wall with progressive surface waves. *J. Fluid Mech.* **41**, 259–281.

KONDO, J. & NAITO, G. 1972 Disturbed wind fields around the obstacle in sheared flow near the earth's surface. *J. Meteor. Soc. Japan*, to be published.

KONDO, J., NAITO, G. & FUJINAWA, Y. 1971 Response of cup anemometer in turbulence. *J. Meteor. Soc. Japan*, **49**, 63–74.

LAMB, H. 1945 *Hydrodynamics*. Dover.

LIGHTHILL, M. J. 1957 The fundamental solution for small steady three-dimensional disturbances to a two-dimensional parallel shear flow. *J. Fluid Mech.* **3**, 113.

LIGHTHILL, M. J. 1962 Physical interpretation of the mathematical theory of wave generation by wind. *J. Fluid Mech.* **14**, 385–398.

LUMLEY, J. L. & PANOFSKY, H. A. 1964 *The Structure of Atmospheric Turbulence*, p. 239. Wiley.

MILES, J. W. 1957 On the generation of surface waves by shear flows. *J. Fluid Mech.* **3**, 185–204.

NAN'NITI, T., FUJIKI, A. & AKAMATSU, H. 1968 Micro-meteorological observations over the sea. Part 1. *J. Oceanogr. Soc. Japan*, **24**, 281–294.

PHILLIPS, O. M. 1966 *The Dynamics of the Upper Ocean*, p. 261. Cambridge University Press.

POND, S., STEWART, R. W. & BURLING, R. W. 1963 Turbulence spectra in the wind over waves. *J. Atmos. Sci.* **20**, 319–324.

POND, S., SMITH, S. D., HAMBLIN, P. E. & BURLING, R. W. 1966 Spectra of velocity and temperature fluctuations in the atmospheric boundary layer over the sea. *J. Atmos. Sci.* **23**, 376–386.

ROLL, H. U. 1965 *Physics of the Marine Atmosphere*, p. 246. Academic.

SHEMDIN, O. H. & HSU, E. Y. 1966 The dynamics of wind in the vicinity of progressive water waves. *Dept. of Civil Engng Tech. Rep. Stanford University*, no. 66.

STEWART, R. H. 1970 Laboratory studies of the velocity field over deep-water waves. *J. Fluid Mech.* **42**, 733–754.

TAKEDA, A. 1963 Wind profiles over sea waves. *J. Oceanogr. Soc. Japan*, **19**, 16–22.

WEILER, H. S. & BURLING, R. W. 1967 Direct measurements of stress and spectra of turbulence in the boundary layer over the sea. *J. Atmos. Sci.* **24**, 653–664.

WU, J. 1968 Laboratory studies of wind–wave interaction. *J. Fluid Mech.* **34**, 91–111.

YEFIMOV, V. V. & SIZOV, A. A. 1969 Experimental study of the field of wind velocity over waves. *Izv. Atmos. Oceanic Phys.* **5**, 930–942.